International Journal of Nanomedicine

Dovepress
open access to scientific and medical research

Open Access Full Text Article

ORIGINAL RESEARCH

Influence of Different Ratios of DSPE-PEG2k on Ester Prodrug Self-Assembly Nanoparticles for Cell Migration and Proliferation Suppression

Huiyun Zhang[1], Shunru Wei[1], Yunfei Hu[1], Yu Zhang[1], Hao Yao[1], Gang Qi[1], Michael Adu-Frimpong[2], Congyong Sun[3]

[1]Department of Pharmaceutical Engineering, School of Chemistry and Chemical Engineering, Yancheng Institute of Technology, Yancheng, Jiangsu, 224003, People's Republic of China; [2]Department of Biochemistry and Forensic Sciences, School of Chemical and Biochemical Sciences, C. K. Tedam University of Technology and Applied Sciences (CKT-UTAS), Navrongo, UK-0215-5321, Ghana; [3]Department of Central Laboratory, The Affiliated Huaian No.1 People's Hospital, Nanjing Medical University, Huai'an, Jiangsu, 223300, People's Republic of China

Correspondence: Michael Adu-Frimpong; Congyong Sun, Email madufrimpong@cktutas.edu.gh; cysun_hayy@163.com

Background: Bufalin (BFL, an active anti-tumor compound derived from *toad venom*) is limited in its application due to high toxicity and rapid metabolism of the cardiotonic steroid. Ester prodrug self-assembly nanoparticles have shown significant improved effects in addressing the above-mentioned issues.

Methods: An ester bond was formed between linoleic acid and bufalin to synthesize linoleic acid-bufalin prodrug (LeB). The self-assembly nanoparticles (LeB-PSNs) containing different mass ratios of DSPE-PEG2k and prodrug (6:4, 7:3, 8:2, 9:1 and 10:0) were prepared via co-precipitation method and defined as 6:4-PSNs, 7:3-PSNs, 8:2-PSNs, 9:1-PSNs and LeB-PSNs, respectively. Further, the characterization (particle size, zeta potential, surface morphology and stability) of the nanoparticles was carried out. Finally, we evaluated the impact of different ratios of DSPE-PEG2k on the hydrolysis rate, cytotoxicity, cellular uptake, cell migration and proliferation suppression potential of the prodrug nanoparticles.

Results: The linoleic acid-bufalin prodrug (LeB) was successfully synthesized. Upon the addition of DSPE-PEG2k at different weight ratios, both particle size and polydispersity index (PDI) significantly decreased, while the zeta potential increased remarkably. No significant differences in particle size, PDI and Zeta potential were observed among the 9:1, 8:2 and 7:3 PSNs. Notably, the 8:2 (w/w) DSPE-PEG2k nanoparticles exhibited superior stability, hydrolysis and cellular uptake rates, along with efficient cell cytotoxicity, cell migration and proliferation suppression.

Conclusion: These findings indicate that DSPE-PEG2k could improve the performance of BFL prodrug nanoparticles, namely enhancing stability and achieving adaptive drug release by modulating the hydrolysis rate of esterase. This study therefore provides more opportunities for the development of BFL application.

Keywords: bufalin, prodrug nanoparticles, DSPE-PEG2k, esterase hydrolysis rate

Introduction

Bufalin (BFL), a naturally occurring compound derived from the venom of the Chinese toad, has been widely explored for its clinical potential in the treatment of various types of cancers, including liver, stomach, lung, colorectal, esophageal, pancreatic cancer, and acute leukemia.[1–3] In vitro studies have demonstrated that BFL exhibits over multiple times greater anticancer efficacy compared to clinical anticancer drugs such as paclitaxel, doxorubicin, and vinblastine while exhibiting relatively lower toxicity towards normal cells.[4] The anticancer mechanism of BFL involves the modulation of multiple signaling pathways, including PI3K/Akt, NF-κB, and Wnt, thereby culminating in suppression of tumor cell growth and metastasis.[5–8] Additionally, BFL exerts its antitumor effects through mechanisms such as cell cycle regulation, angiogenesis inhibition, and immune modulation.[9,10] Furthermore, bufalin could reverse different tumor cell resistance through multiple mechanisms and have a good synergistic therapeutic effect with other clinical

Received: 21 November 2023
Accepted: 12 March 2024
Published: 18 March 2024

Graphical Abstract

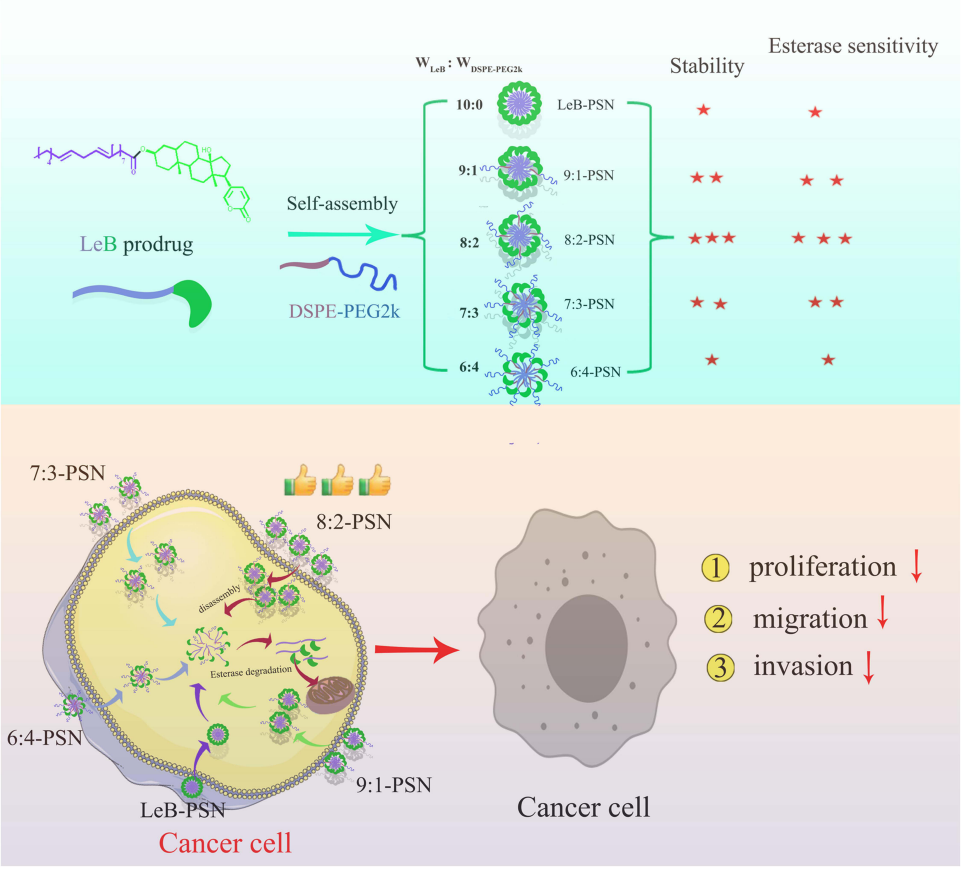

chemotherapy drugs such as cisplatin, paclitaxel, sorafenib and gefitinib.[11–13] Bufalin could enhance paclitaxel-induced apoptosis in breast cancer MCF-7 cells by partially inhibiting AKT activation induced by paclitaxel and upregulating the activity of p38.[13]

However, it is important to note that BFL is known to possess inherent cardiotoxicity, wherein it induces arrythmias at increased dosages[14] and limits its clinical use.[15] In addition, problems such as rapid metabolism and low tumor delivery rate of BFL can also affect the effectiveness of its antitumor effect.[16] Therefore, addressing challenges such as reducing toxicity, improving drug delivery, and enhancing bioavailability are critical for further development and clinical application of BFL.

Ester prodrug design represents a crucial strategy in drug development, offering broad potential for enhancing drug efficacy and safety.[17] This approach finds extensive application prospects in pharmaceutical research, thus aiming to mitigate drug toxicity and achieve controlled release of the active compound.[18,19] It is said that when a drug is converted into an ester precursor form, its inherent activity is suppressed until specific enzymatic catalysis triggers its transformation into the active drug within the body.[20] This controlled release mechanism minimizes adverse effects on healthy tissues, thereby reducing the risk of drug toxicity.[21] Additionally, ester prodrug design holds promise for improving the pharmacokinetic properties of drugs.[22] Addressing challenges such as premature hydrolysis of the ester precursor within the body and ensuring selective release of the drug in tumor cells are essential considerations.[23] Overall, incorporation of ester prodrug design in drug development provides avenues to optimize drug performance and expand therapeutic capabilities.

In order to address issues associated with ester prodrugs, researchers have employed prodrug self-assembling nanotechnology.[24] Prodrug self-assembling nanodelivery is a "self-loading and self-delivering" high-capacity delivery system. Nonetheless, the hydrophobic nature of the linoleic acid ester bond-prodrug nanoparticles can lead to rapid clearance in vivo.[25] Indeed, PEGylation with DSPE-PEG2k is necessary to enhance the stability and circulation time of ester prodrugs in vivo. However, preliminary findings suggest that the presence of DSPE-PEG2k also has significant impact on esterase activity and the hydrolysis rate of ester prodrugs. Therefore, this study prepared linoleic acid ester bond-bufalin prodrug/DSPE-PEG2k self-assembly nanoparticles (LeB/DSPE-PEG2k-PSNs) with varied mass ratios (6:4, 7:3, 8:2 and 9:1) and investigated the differences in stability and hydrolysis rates among various prepared LeB/DSPE-PEG2k-PSNs, as well as their effects on cell proliferation, uptake, migration, and invasion. These findings may provide valuable insights for the clinical application of BFL ester prodrugs.

Materials and Methods

Materials

The BFL was purchased from Baoji Biotechnology Co., Ltd, (Shanxi, China). Aladdin Industrial Corp., (Shanghai, China) provided 4-dimethyl-aminopyridine (DMAP), acetic anhydride and dicyclohexyl-carbodiimide (DCC), while AVT pharmaceutical Co. Ltd. (Shanghai, China) supplied 1, 2-distearoyl-sn-glycero-3-phospho-ethanol-amine -N-[methoxy-ethylene-glycol)-2000] (DSPE-PEG2k). We obtained dithiodiglycolic acid, linoleic acid and ethylene glycol from MACKLIN Scientific Co., Ltd. (Shanghai, China). Invitrogen (Carlsbad, CA, USA) supplied Dulbecco's Modified Eagle's medium (DMEM) and fetal bovine serum (FBS), while Sinopharm Chem. Reagent Co. Ltd. (Shanghai, China) provided acetonitrile and methanol (chromatographically pure). Human esophageal cancer cell (KYSE-150) and healthy epidermal epithelial cells (HEEC) were purchased from Bena Culture Collection (Suzhou, China).

Synthesis and Characterization of LeB Prodrug

A mixture of linoleic acid (28 mg, 0.1 mmol), DCC (24 mg, 0.12 mmol), DMAP (15 mg, 0.13 mmol), and BFL (50 mg, 0.1 mmol) was dissolved in anhydrous dichloromethane (6 mL). The reaction mixture was stirred under sealed conditions for 24 hours. After filtration, the reaction solution was purified through silica gel column chromatography, using an elution ratio of dichloromethane/methanol (30/1, v/v). A white solid was obtained (30 mg), which corresponded to a yield of 40.3%. The target product was characterized and confirmed via nuclear magnetic resonance (NMR) spectroscopy (AVANCE III HD, Bruker, Switzerland) and mass spectrometry (MS, Agilent 1290–6545, Agilent, USA).

Preparation of PSNs

In brief, we followed these steps to prepare nanoparticles using a one-step nanoprecipitation method.[26] Firstly, the LeB prodrug was mixed with anhydrous ethanol to prepare a solution with a total concentration of 10 mg/mL. Under stirring conditions, 400 μL of the prodrug anhydrous ethanol solution was slowly added dropwise into 4 mL of double-distilled water. The ethanol was then removed by rotary evaporation, followed by the addition of water to bring the final volume to 4 mL, thus resulting in the formation of self-assembled nanoparticles of LeB prodrug (LeB-PSN). The same method was applied to produce LeB/DSPE-PEG2k prodrug self-assembled nanoparticles with varied mass ratios (6:4, 7:3, 8:2 and 9:1). The only difference is that varying proportions of DSPE-PEG2k were added to the LeB anhydrous ethanol solution. These compositions were, respectively, defined as 9:1-PSN, 8:2-PSN, 7:3-PSN and 6:4-PSN.

Characterization of PSNs

Particle size and zeta potential are measured using a dynamic light scattering-based nanoparticle size analyzer (Malvern particle size and zeta potential analyzer, Malvern, Britain). Dilution of the prepared nanoparticles to a concentration of 0.2 mg/mL was carried out with ultrapure water. Later on, we carried out appropriate analysis, namely determination of the intensity distribution, polydispersity index (PDI) and zeta potential. Transmission electron microscopy (TEM, JEM-1400, JEOL, Tokyo-Japan) was utilized to examine the size and surface morphology of the nanoparticles. Aliquot of diluted nanoparticles (0.1 mg/mL) was deposited onto a copper grid, followed by infrared drying. Subsequently,

a phosphotungstic acid-negative staining solution was applied for 1 minute, while excess stain was removed. After air- and static drying, the copper grid was examined under the TEM to observe and document the morphological features of the nanoparticles. The determination of critical micelle concentration (CMC) was described in the Supplementary Material 1.

Stability Analysis of PSNs

The colloidal stability of the synthesized nanoparticles was assessed over an extended period using a two-step method. Firstly, the long-term colloidal stability was examined in water at a temperature of 4°C and 25 °C, over a duration of 30 days. Additionally, we evaluated the nanoparticles' stability in phosphate-buffered saline (PBS, pH=7.4) over a shorter timeframe of 24 hours at a temperature of 37 °C. At predetermined time intervals, we determined the size of the nanoparticles under the same conditions as described in section 2.4.

In vitro Release Evaluation

The in vitro release of BFL from PSNs was studied using pH=7.4 PBS as the release medium at 37 °C, with or without 50 U pig liver esterase. The PSNs (0.5 mL, 1 mg/mL) were placed in a 9.5 mL of release medium. Samples (0.2 mL) were collected at specific time intervals (0, 0.5, 1, 3, 6, 12, 24 and 48 hours). Analysis of each collected sample was performed with high performance liquid chromatographic (HPLC) technique at every time point by mixing the sample with 0.6 mL of methanol. Afterwards, we calculated the cumulative release percentage on the basis of ratio of BFL released to theoretically loaded amount in PSNs.

Evaluation of Cell Viability of PSNs

The cell viability of PSNs on KYSE-150 cells was evaluated using the 3-(4,5-dimethyl-thiazol-2-yl)-2,5-diphenyl-tetrazolium bromide (MTT) assay for 72 hours, following a previously described method by Zhang et al.[27] Specifically, we treated KYSE-150 cells with 100 μL of culture medium comprising varied drug samples (free BFL and various PSNs) at various concentrations (0.5, 1, 5, 10, 25, 50, 100, 200 and 400 nM). Afterwards, we calculated the rate of cell viability through the following equation: VR (%) = A/A1 × 100%, wherein A represents treated group absorbance and A1 denotes vehicle control group absorbance.

Evaluation of in vitro Cell Uptake of PSNs

The cell uptake of PSNs was evaluated using fluorescence microscopy after we have incorporated the fluorescent dye coumarin-6 (C-6). Seeding of KYSE-150 cells was performed in 6-well plates at 1×10^6 cells/well density before incubation in DMEM medium which has been supplemented with FBS (10%), penicillin (100 U/mL), and streptomycin (100 μg/mL). Pre-incubation was performed for 24 hours, after which we washed the cells before incubation for 0.5 or 3 hours with either C-6@PSNs or free C-6 solution (comprising 0.1% Tween 80), wherein the dosage forms contained an equivalent C-6 concentration (50 ng/mL). After incubation, we used ice-cold PBS (pH=7.4) to wash the cells thrice. Later on, we, respectively, fixed the cells and stained their nuclei with DAPI. Observation of the cells with a fluorescence microscope (DMi8, Leica, Germany) was carried out after we have further washed them with PBS.

Cell Scratch Assay

First, we seeded KYSE-150 cells in a 6-well plate at 1×10^5 cells/well density, thereby allowing them to form a fully confluent monolayer. Then, a sterile 10 μL pipette tip was used to create a linear scratch or wound on the cellular monolayer, which generated a gap. After scratching, the cells were gently washed three times with PBS solution to remove any debris or detached cells. Next, the cells were cultured in wells with serum-free medium containing free BFL (13 nM) or different nanoparticles (PSNs, 13 nM, the equivalent dose for BFL). The cells were further cultured for 24 and 48 hours, before we observed and captured the migration distance of cells in varied groups.

Migration and Invasion Assay

In the migration assay, we suspended KYSE-150 cells (2×10^3 cells/well) in serum-free DMEM prior to addition to upper chamber of a Transwell plate with 8 μm pores. Afterwards, PBS, BFL and different PSNs treatments were added at a final concentration of 13 nM. The lower chamber was filled with DMEM containing 10% FBS. Later, the plate was incubated in a cell culture incubator for 48 hours. After removing the insert, the membrane was carefully detached and fixed. Crystal violet staining was performed, while the migrated cells were counted under a microscope in at least three randomly selected fields. The cell count was averaged for each field. Based on the migration assay protocol, we performed the invasion assay using Matrigel-coated Transwell inserts.

The Pharmacokinetic Analysis in Rats

The methods of pharmacokinetic analysis in rats were provided in Supplementary Material 1.

Statistical Analysis

Analysis was performed using GraphPad Prism 10.1.2 software. Statistical analysis between groups was performed using two-tailed Student's *t*-test and one-way ANOVA, where ns indicates no significance, $P < 0.05$ was considered statistically significant, whereas $p < 0.01$ was regarded as highly significant.

Results and Discussion

Synthesis and Structure Confirmation of LeB Prodrug

The LeB prodrug was synthesized through an esterification reaction between BFL and linoleic acid (Figure 1A). The structure of the LeB prodrug was confirmed by NMR and MS analysis. The chemical formula of the target compound LeB prodrug is $C_{42}H_{64}O_5$. ESI-MS (-): m/z: 693.4720 [M+HCOO]-(Figure S1) ^{1}H-NMR (400 MHz, $CDCl_3$): 7.86 (1H, dd, J=9.7, 2.6), 7.25 (1H, d, J=9.0), 6.26 (1H, dd, J=9.7, 0.7), 5.47–5.25 (4H, m), 5.23–4.86 (1H, m), 2.84–2.58 (2H, m), 2.54–2.41 (1H, m), 2.36–1.99 (8H, m), 0.96 (3H, s, H-19), 0.89 (3H, t, LA-CH3), 0.70 (3H, s, H-18) ^{13} C-NMR (400 MHz, $CDCl_3$): 173.36, 162.42, 148.53, 146.89, 130.20, 130.01, 128.03, 127.89, 122.75, 115.25, 85.26, 77.38, 77.27, 77.07, 76.75, 70.04, 51.21, 48.36, 42.29, 40.84, 36.89, 35.82, 35.14, 34.79, 32.75, 31.51, 30.51, 30.46, 29.59, 29.33, 29.19, 29.14, 29.11, 28.74, 27.18, 26.41, 25.62, 25.11, 25.08, 23.76, 22.56, 21.41, 21.29, 16.54, 14.08. The changes in

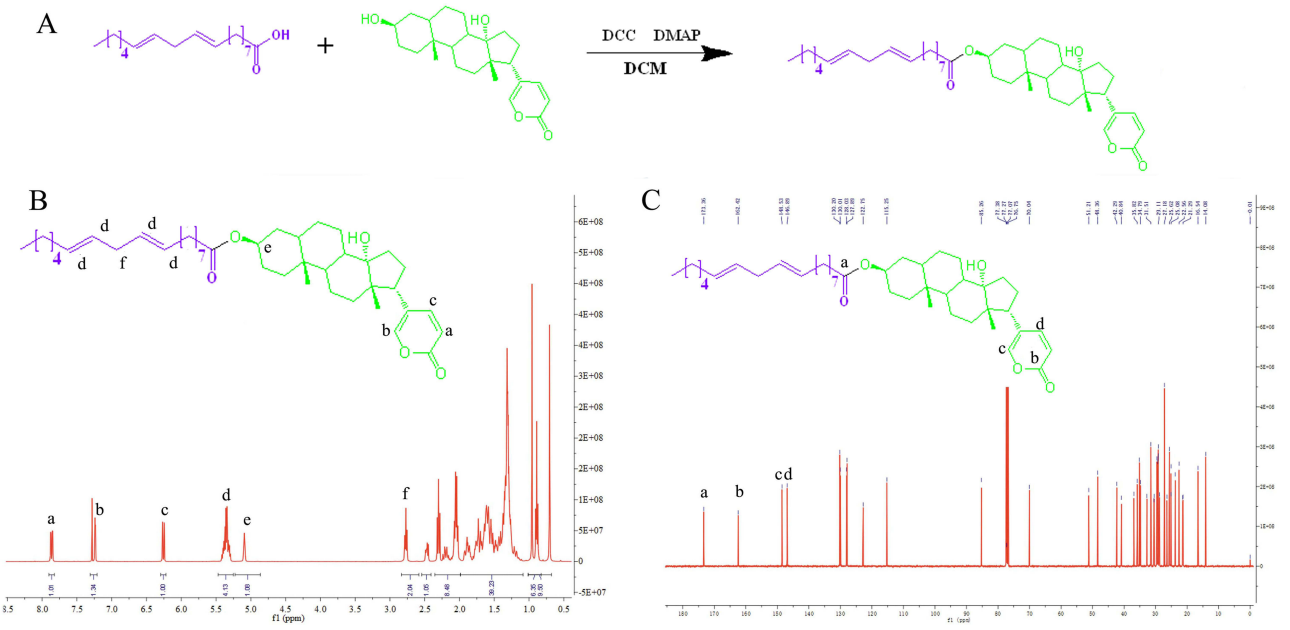

Figure 1 The synthetic route and nuclear magnetic resonance (NMR) characterization of the prodrug. (**A**) Schematic representation of the synthesis route of the prodrug. NMR spectra of the prodrug, including the hydrogen spectrum (**B**) and the carbon spectrum(**C**).

chemical shift of H3 and C3 in BFL structure indicate that the prodrug was synthesized through the esterification reaction between linoleic acid and BFL at the C3-OH group (Figure 1B and C). Hence, we affirmed successful synthesis of the prodrug with the above results.

Physical Characterization of LeB-PSN and LeB/DSPE-PEG2k-PSNs

The LeB-PSN nanoparticles were prepared using a nanoprecipitation method, wherein LeB/DSPE-PEG2k-PSNs with different weight ratios of DSPE-PEG2k (6:4, 7:3, 8:2 and 9:1) were also synthesized. Respectively, laser diffraction and Zeta potential measurements were conducted to determine size of particles and surface charge of the nanoparticles (Figure 2). The results showed that the average particle size of LeB-PSN was approximately 125 nm with a PDI of around 0.147 and a surface charge of −35 mV. The critical micelle concentration of LeB-PSN was 0.002958 mg/mL (Figure S2), which was lower than that of general polymer materials.[28] The low critical micelle concentration also ensures its good stability in water. Once a prodrug undergoes self-assembly into nanoparticles and is subsequently subjected to centrifugation at 5000 rpm for the removal of any precipitates, the measured proportion of actual drug loading obtained through the liquid phase method is in close agreement with the proportion of actual drug content after lyophilization (as indicated in Table S1).

Upon addition of DSPE-PEG2k at different weight ratios, both the particle size and PDI significantly decreased, while the zeta potential increased remarkably. Corroboratively, earlier work has observed a decrease in particle size after PEGylation of prodrug nanoparticles.[29] Specifically, the particle size was discovered to be around 110 nm, while the PDI was approximately 0.12 with surface charge being about −17 mV. No significant differences were observed when particle size, PDI and Zeta potential of 9:1, 8:2 and 7:3 PSNs were compared. However, the 6:4 PSNs exhibited an increase in both particle size, PDI and Zeta potential (Figure 2F–H). TEM analysis revealed that the nanoparticles exhibited

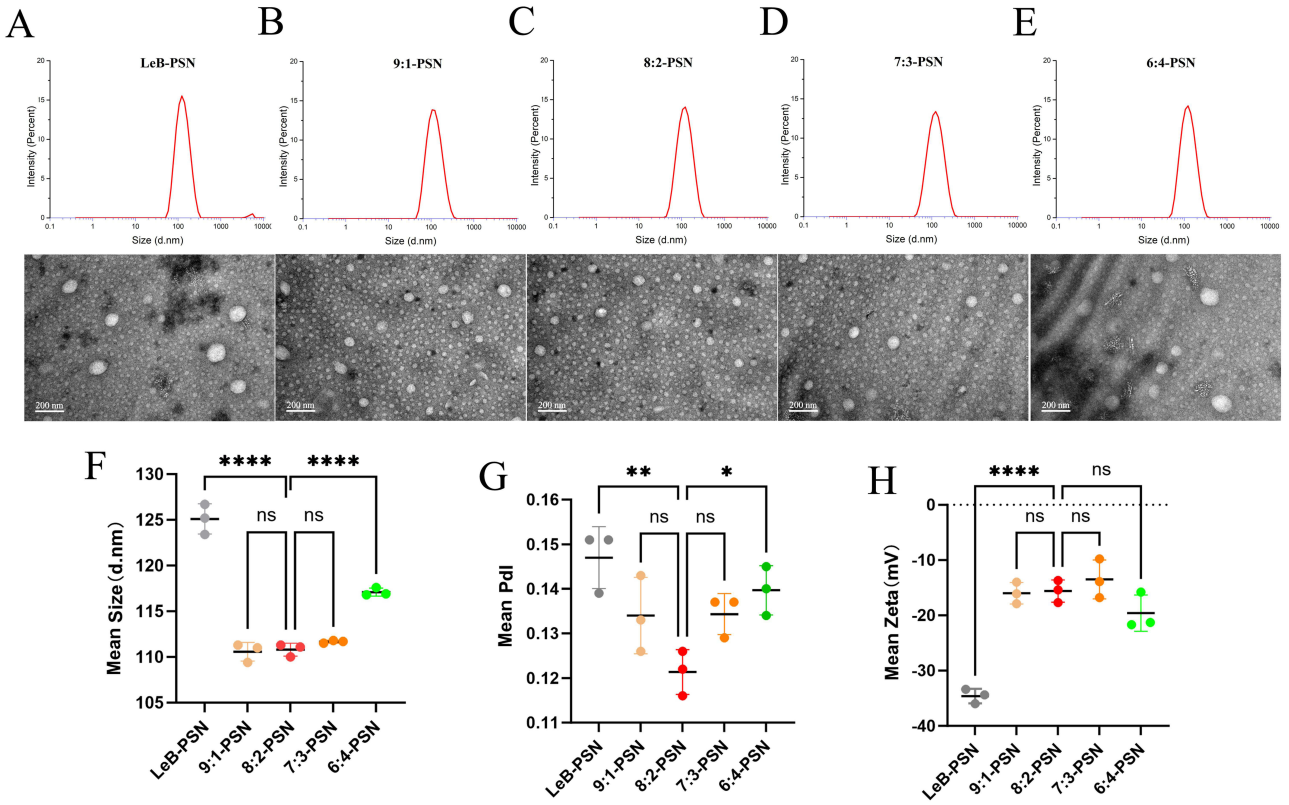

Figure 2 The particle size distribution, polydisperse index (PDI), Zeta potential, and transmission electron microscopic (TEM) images of different nanoparticles. (**A**–**E**) Particle size distribution and TEM images of Leb-PSN, 9:1-PSN, 8:2-PSN, 7:3-PSN, and 6:4-PSN; (**F**–**H**) Average particle size, PDI, and Zeta potential values of Leb-PSN, 9:1-PSN, 8:2-PSN, 7:3-PSN, and 6:4-PSN. Data are presented as mean ± SD, n=3. One-way ANOVA (one-sided) with Dunnett's multiple comparisons test was used for data analysis, where ns indicates no significance, *P < 0.05, **P < 0.01, and ****P < 0.0001.

a spherical morphology that was consistent with the DLS results (Figure 2A–E). Previous reports have indicated that nanoparticles that have sizes ranging 50–200 nm increasingly and progressively accumulate in the extra-vascular compartment of tumor tissues through enhanced permeability and retention (EPR) effect, wherein our prepared nanoparticles fell within this size range.[30,31] Notwithstanding, a comprehensive study to understand the mechanism underlying the accumulation of LeB/DSPE-PEG2k-PSNs in tumor tissues will be explored in not-too-distant future.

The Stability of the Nanoparticles

To further investigate the stability of the nanoparticles, their behavior at different temperatures (4 and 25 °C) and in PBS (37.5 °C) was examined. Following storage for a duration of 30 days at both 4 and 25 °C, we observed no significant changes in particle size for any of the nanoparticles (Figure 3A and B). This suggests robust long-term stability of the nanoparticles under these storage conditions. However, in PBS (pH=7.4) at 37.5 °C, there was a rapid increase in particle size accompanied by precipitation for LeB-PSN. In comparison, the 8:2-PSN formulation exhibited the smallest particle size when it was exposed to PBS, thus demonstrating a significant difference in comparison to 9:1-PSN (Figure 3C). Furthermore, the PEGylated nanoparticles showed no noticeable changes within 24 hours, which indicate a marked improvement in stability following PEGylation. In 10% FBS solution, 8:2-PSN also exhibited the best stability, with minimal changes in particle size within 24 hours (Figure S3). These findings underscore the substantial advantages of PEGylation in enhancing stability as well as the critical role of optimizing the amount of medium to ensure nanoparticle stability in medical applications.[32] In particular, PEGylation of nanoparticles is usually shielded from aggregation, which in turn can stabilize the nanoparticles upon dispersion.[33]

Esterase Hydrolysis Rate of LeB-PSNs and LeB/DSPE-PEG2k-PSNs

Enzymatic or nonenzymatic hydrolysis of ester prodrugs is very significant for their activation in vivo and in vitro.[34] To simulate this phenomenon, we investigated the drug release behavior of LeB-PSNs and LeB/DSPE-PEG2k-PSNs in PBS solutions with or without 50 U/mL esterase (Figure 4A and B). The results showed no significant difference in the prodrug hydrolysis rate between LeB-PSNs and LeB/DSPE-PEG2k-PSNs in PBS (pH=7.4) without esterase (Figure 4B). However, surprisingly, the drug release rate of LeB/DSPE-PEG2k-PSNs was significantly higher than that of LeB-PSNs in PBS (pH=7.4) with esterase (Figure 4A and C). Among these different LeB/DSPE-PEG2k-PSNs, the cumulative release rates at 48 hours (Figure 4C) and 72 hours (Figure S4) of 8:2-PSN were markedly higher compared to other ratios of PSNs. To exclude the influence of DSPE-PEG2k solubilization, we further examined the situation with the addition of 0.1% Tween 80 and 0.002% DSPE-PEG2k (the same DSPE-PEG2k content as in 8:2-NPs) in the medium (Figure 4D). The results showed that the drug release rate of LeB-PSNs decreased, possibly due to the addition of surfactant (Tween 80), which increased the stability of the nanoparticles. Therefore, the increase in drug release rate of LeB/DSPE-PEG2k-PSNs was not caused by DSPE-PEG2k solubilization. The possible reason may be that the esterase degraded DSPE-PEG2k, thereby disrupting the intermolecular balance within the nanoparticles,[16,35] which led to increased prodrug

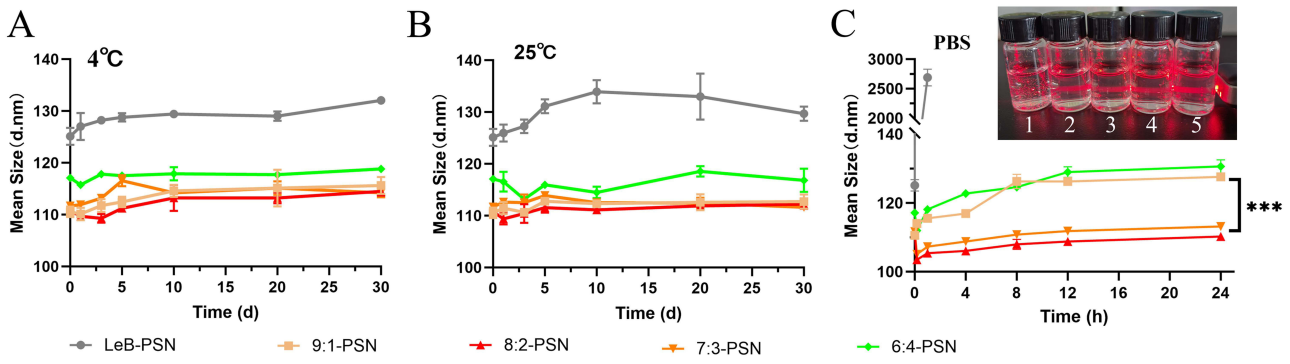

Figure 3 The particle size variation of different nanoparticles after storage at 4°C (**A**) and 25°C (**B**) for 30 days, and stability assessment in phosphate-buffered saline (PBS, pH 7.4) over 24 hours (**C**). Insert: the Tyndall effect image with different nanoparticles of Leb-PSN (1), 9:1-PSN (2), 8:2-PSN (3), 7:3-PSN (4) and 6:4-PSN (5) under direct laser beam irradiation. Data are presented as mean ± SD, n=3. Statistical analysis was performed using two-tailed Student's *t*-test, ***$P < 0.001$.

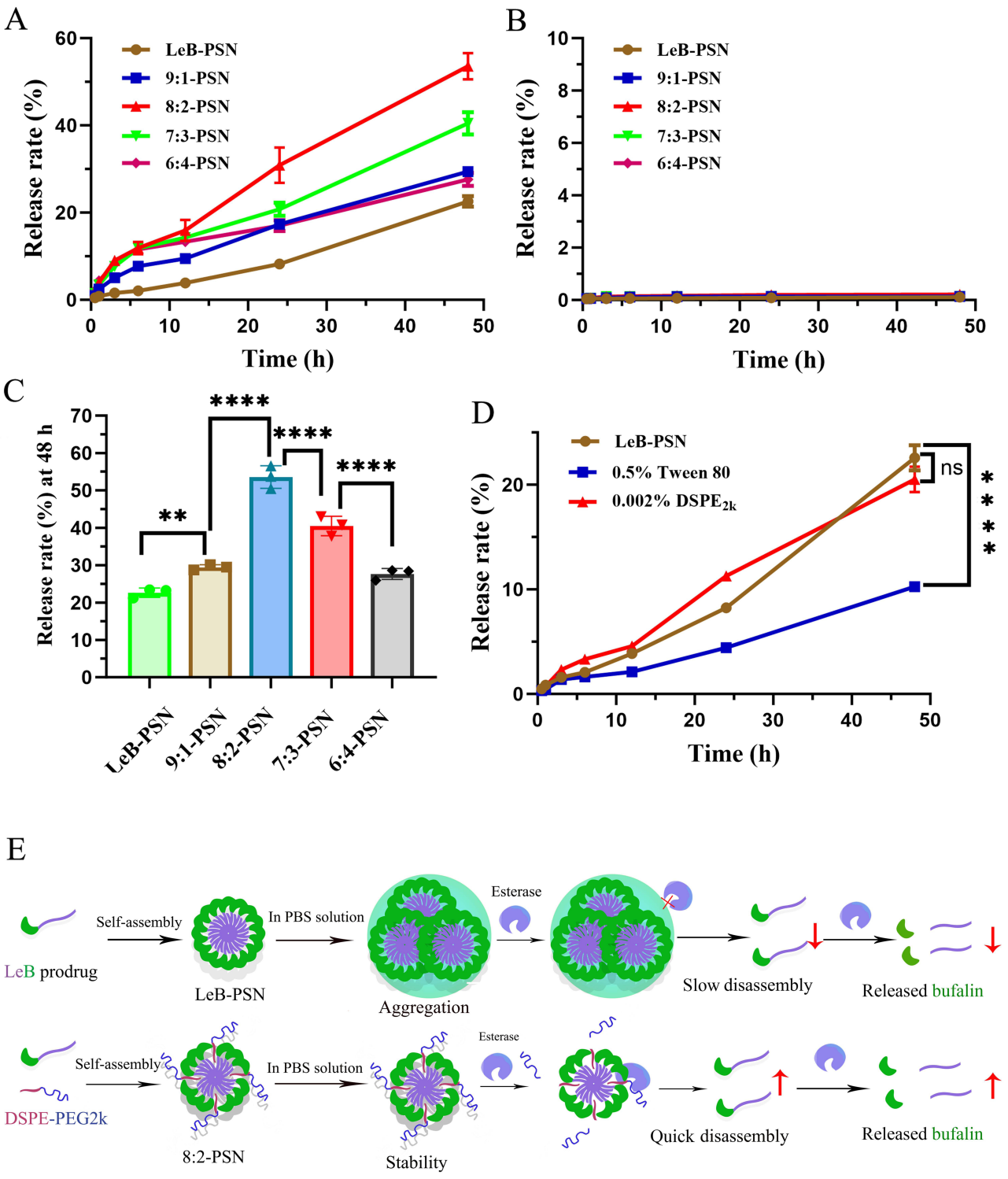

Figure 4 The drug release profiles of different nanoparticles under enzymatic (**A**) and non-enzymatic conditions (**B**). Release percentages of different nanoparticles after 48 hours under enzymatic conditions (**C**). One-way ANOVA (one-sided) with Dunnett's multiple comparisons test was used for data analysis. (**D**) Drug release profiles of LeB-PSN in media containing Tween 80 and DPSE2k. Statistical analysis was performed using two-tailed Student's *t*-test, where ns indicates no significance, $^{**}P < 0.01$, and $^{****}P < 0.0001$. (**E**) Schematic representation of the drug release mechanism of nanoparticles under enzymatic conditions.

release and subsequently accelerated drug release rate (Figure 4E). In support of the above findings, available literature has indicated that hydrolysis of ester linkages results in increased drug release.[36] In addition, after PEG modification, the hydrophilicity of the nanoparticle surface increased, thus weakening the hydrophobic interaction with esterase.[37] However, after PEG had completely covered the nanoparticle surface, it may have protected the ester bond. This explains why further increase in DSPE-PEG2k content led to a slower release rate

The strategy of increasing the selective cytotoxicity of drugs by harnessing the release properties sensitive to esterase has garnered extensive attention and application in tumor treatment research.[35,38] The in vitro release results of 8:2-PSN exemplify its propensity for esterase-sensitive liberation. Due to the relatively higher esterase levels in tumor cells compared to normal cells, 8:2-PSN could be rapidly disassembled and subsequent released the LeB prodrug within tumor cells. Moreover, the prodrug would undergo hydrolysis by esterase, thus yielding the prototype active pharmaceutical agent.[39] Simultaneously, owing to the comparably reduced esterase levels in normal cells, the hydrolysis of the LeB prodrug is less pronounced, thus resulting in a relatively diminished toxicity towards normal cells.[40] Consequently, through its esterase-sensitive release characteristics, 8:2-PSN can showcase heightened selectivity towards tumor cells while mitigating deleterious effects on normal cells.

Cell Cytotoxicity Bioactivation

We conducted a study on the cytotoxicity of BFL on KYSE150 cells (Figure 5A). The cell cytotoxicity of paclitaxel on KYSE150 cells is provided in Figure S5. The half-maximal inhibitory concentration (IC_{50}) of paclitaxel on KYS150 cells at 24, 48 and 72 hours was 572 nM, 173 nM and 92 nM, respectively. In contrast, the IC_{50} of BFL on KYSE150 cells at 24, 48 and 72 hours was 49.3 nM, 4.7 nM and 2.9 nM, respectively. These findings suggest that BFL exhibited superior toxic effects compared to paclitaxel (Figure S6), which aligned with the consistent outcomes reported in other scholarly literature.[41] Additionally, we tested the inhibitory effect of Leb-PSN and Leb/DSPE-PEG2k-NPs with different mass ratios on KYSE150 cell proliferation (Figure 5B–F). The IC_{50} of different PSNs is shown in Figure 5G. The results revealed that these nanoparticles had significantly lower inhibitory effects on KYSE150 cell proliferation compared to free BFL. Specifically, at different time points (24, 48 and 72 hours), the 8:2-PSN formulation showed the best inhibitory effect on KYSE150 cells, while the non-PEGylated LeB-NPs exhibited the weakest cytotoxicity. These results are consistent with our earlier findings regarding stability and in vitro release experiments. Therefore, we speculated that these differences may be related to the stability of different PEGylated drug nanoparticles and their response to esterase. Additionally, these discrepancies may also be influenced by the cell uptake rates of nanoparticles in different cells.[42]

In order to validate the selectivity of different PSNs towards tumor cells, we also examined the cytotoxicity on healthy epidermal epithelial cells (HEEC). The results, as shown in Figure S7, indicated that the cytotoxicity of the PSNs was significantly lower than that of free BFL at 24 and 48 hours. Furthermore, the relative cytotoxicity (the ratio values of IC_{50} to HEEC and KYSE150) was significantly enhanced (Table S2). Remarkably, the relative cytotoxicity value was highest for 8:2-PSN at 48 hours. This observation may be attributed to the heightened hydrolysis degree of 8:2-PSN within tumor cells, which was induced by their superior esterase sensitivity.

Cellular Uptake Bioactivation

According to the results of cytotoxicity, PEGylated prodrug nanoparticles exhibited significantly higher cell cytotoxicity compared to non-PEGylated prodrug nanoparticles. Cellular uptake is an important factor influencing the efficacy of prodrugs as they need to enter tumor cells and undergo conversion into active drugs. To assess cellular uptake, we labeled the prodrug nanoparticles with a fluorescent substance (C-6), wherein the fluorescence intensity within the cells was used to reflect the extent of nanoparticle uptake. After 1 hour of administration, the 8:2-PSN group displayed significantly higher fluorescence intensity compared to other groups (Figure 6A). At 6 hours, the 8:2-PSN group exhibited the highest fluorescence intensity, which was significantly greater than the other groups (Figure 6B).

There are several factors that influence cellular uptake. For free drug, it is closely related to their physicochemical properties. Herein, free C-6 was primarily absorbed through passive diffusion for transmembrane transport.[43] However, in the case of nanocarrier systems, there are additional factors that can affect cellular uptake, namely particle size, surface charge, and drug release rate.[44] In our experiments, we did not observe significant differences in particle size and surface

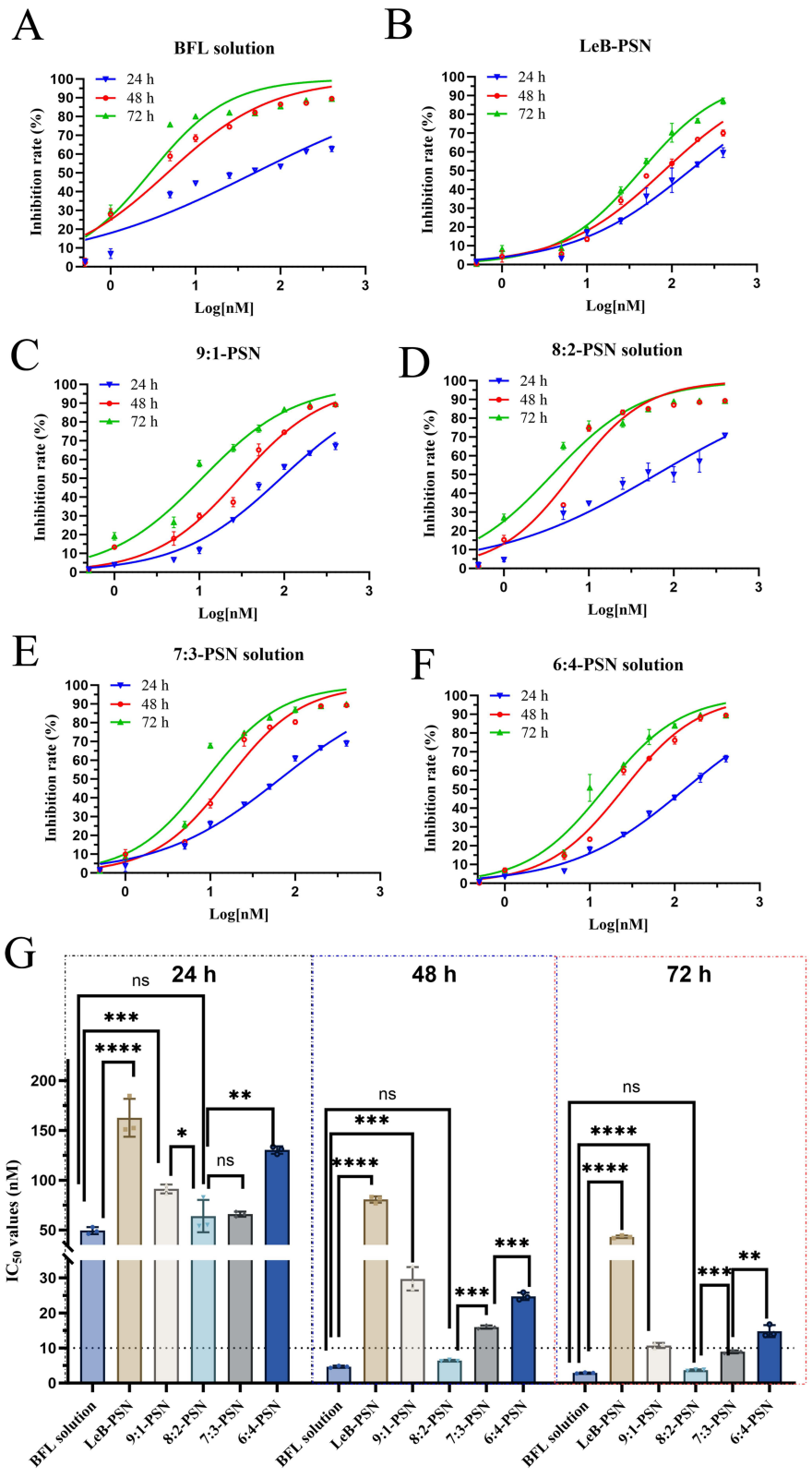

Figure 5 The cytotoxicity of Bufalin (BFL) and different nanoparticles on KYSE150 cells. (**A**–**F**) The cytotoxicity of free BFL solution, Leb-PSN, 9:1-PSN, 8:2-PSN, 7:3-PSN, and 6:4-PSN at different time points (24, 48, and 72 hours). (**G**) The IC_{50} values of different nanoparticles on KYSE150 cells at different time points (24, 48, and 72 hours). One-way ANOVA (one-sided) with Dunnett's multiple comparisons test was used for data analysis, where ns indicates no significance, *P < 0.05, **P < 0.01, ***P < 0.001, and ****P < 0.0001.

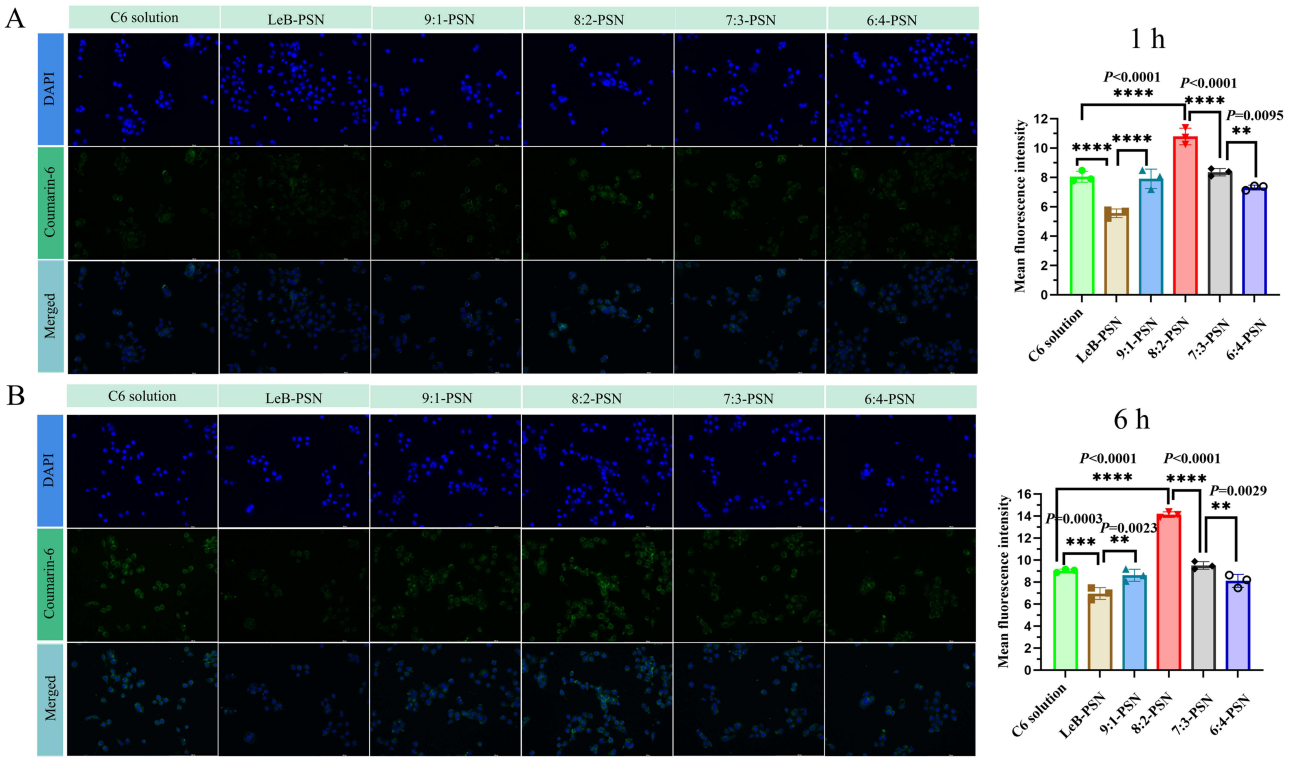

Figure 6 The cell uptake in KYSE150 cells. The fluorescence intensity images were obtained using a fluorescence microscope and the fluorescent intensity values were calculated using the Image software at 1hours (**A**) and 6 hours (**B**) after treatment with various nanoparticles on KYSE150 cells. Statistical analysis was performed using two-tailed Student's *t*-test, where **P < 0.01, ***P < 0.001, and ****P < 0.0001.

charge between 9:1-PSNs, 8:2-PSNs, and 7:3-PSNs. Nevertheless, the cellular uptake results showed significant differences (Figure 6B). This disparity could be attributed to two main factors: firstly, differences in stability.[45] In particular, 8:2-PSN group exhibited the highest stability, with minimal aggregation and enlargement. Secondly, the effect of aggregation quenching due to drug release rate.[46] The 8:2-PSN group showed the fastest drug release rate and the least aggregation quenching effect. Even with the presence of aggregation quenching, the fluorescence intensity of the 8:2-PSN group remained significantly higher than that of free C-6, thus indicating a significantly higher proportion of cellular uptake for the 8:2-PSN group. In summary, our experimental results demonstrate the significant advantage of PEGylated prodrug nanoparticles in terms of cellular uptake, with the 8:2-PSN group exhibiting the highest cellular uptake. This finding has important implications for the efficacy of prodrugs and may aid in further optimization of drug delivery system design and performance.

Cell Scratch Inhibition Bioactivation

Esophageal squamous cell carcinoma (ESCC) is a complex disease with multiple etiological factors. Due to late-stage diagnosis or metastasis, the prognosis for most patients is poor. In this study, we investigated the inhibitory effects of different PSNs and free BFL on KYSE150 cell migration. Changes in the scratch area of KYSE150 cells were observed under an inverted phase-contrast microscope at 24 and 48 hours (Figure 7A, D and E). The results displayed a lower number of migrating cells in the scratch area in free BFL solution group compared to blank control group. The ratio of uncovered scratch area (LA/L0) was significantly higher in the free BFL solution group compared to blank control group. In line with other reports, BFL exhibited commendable capacity for inhibiting cellular migration.[47] Among the different PSNs, the 8:2-PSN group had the highest LA/L0 values at both 24 and 48 hours, which were significantly higher than the other ratio groups. Due to its higher cellular uptake and enzymatic degradation rate, the 8:2-PSN retained the cell migration inhibitory ability of free BFL (Figure 7A, D and E).

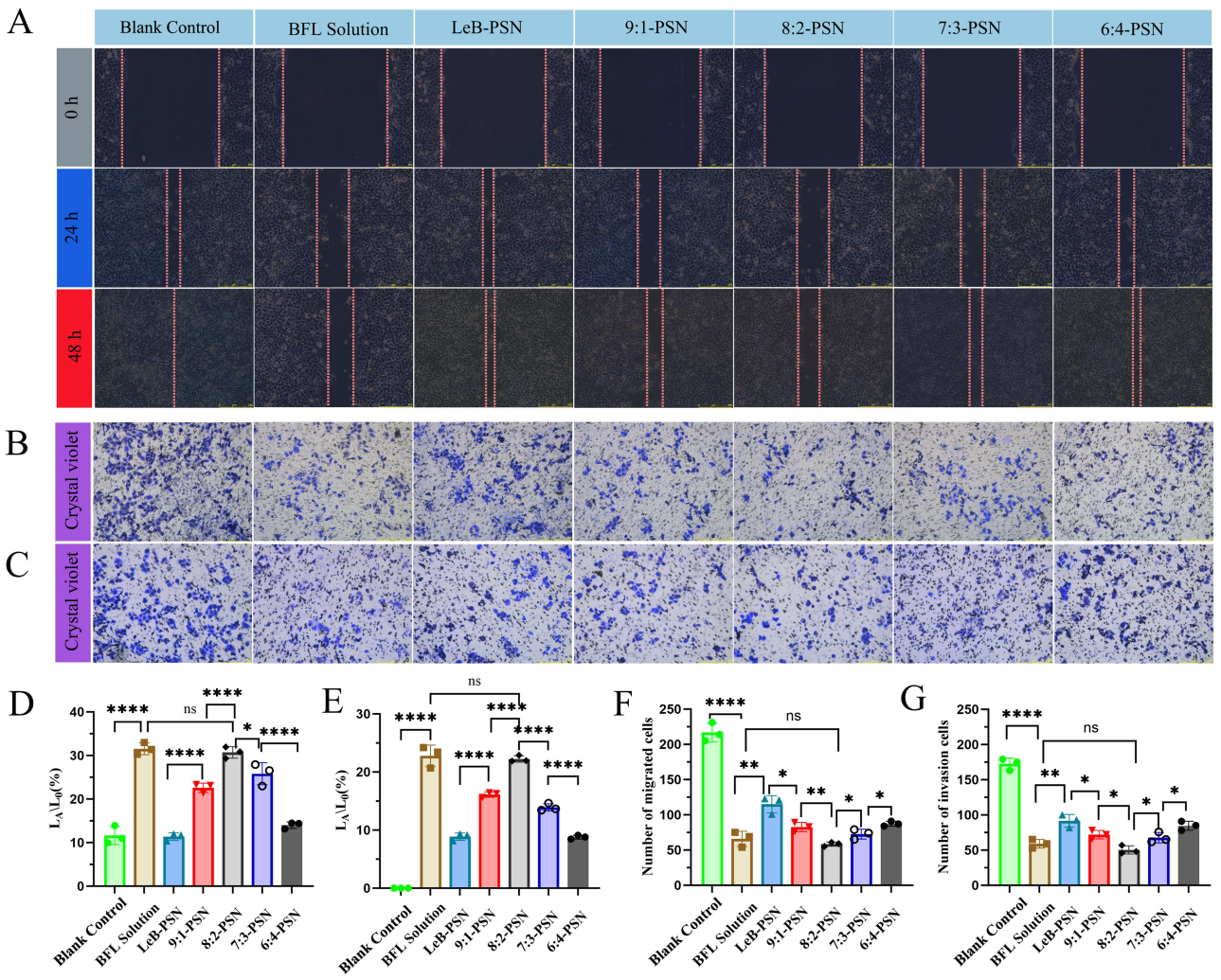

Figure 7 The scratch (**A**), migration (**B**), and invasion (**C**) assays of different nanoparticles on esophageal cancer cells. Changes in the scratch area relative to the blank control group after 24 hours (**D**) and 48 hours (**E**) of nanoparticle treatment. Cell count images of migration (**F**) and invasion (**G**) in different groups after 24 hours of nanoparticle treatment. Statistical analysis was performed using two-tailed Student's *t*-test, where ns indicates no significance, **P* < 0.05, ***P* < 0.01, and *****P* < 0.0001.

Cell Migration and Invasion Inhibition Bioactivation

In order to further investigate the inhibitory effects of BFL and different PSNs on migration and invasion of KYSE150 cell, we employed the Transwell assay. As shown in Figure 7B, C, F, and G, BFL intervention led to a significant inhibition of KYSE150 cell migration and invasion. When compared with different PSNs, the 8:2-PSN group exhibited the highest degree of inhibition on KYSE150 cell migration and invasion, which was significantly superior to other ratio groups. The results showed that the 8:2 PEGylated nanoparticles also retained the cell migration and invasion inhibitory ability of free BFL (Figure 7D–G). These findings are consistent with the results obtained from the cell scratch assay. The enhanced inhibitory effect of the 8:2-PSN group can be attributed to its highest cellular uptake and enzymatic degradation rate, along with better colloidal stability. Relevant studies have suggested that PEGylated nanoparticles are generally able to avoid clearance by phagocytic cells with a longer circulation time and enhanced tumor EPR effect, thereby exhibiting greater potential for application.[48] Therefore, further investigations on in vivo pharmacokinetics were conducted, and the results are shown in Figure S8. The AUC (prodrug in blood) of 8:2-PSN was 110.06 and 218.4-fold higher than free bufalin solution and LeB-PSN, respectively (Table S3). The AUC (bufalin in blood) of 8:2-PSN was 2.64 and 5.40-fold higher than free bufalin solution and LeB-PSN, respectively. Compared to free bufalin solution and LeB-PSN group, the 8:2-PSN group exhibited longer half-life ($t_{1/2}$) due to its superior colloidal stability and PEGylation protection.[49] The aforementioned findings collectively demonstrate that the utilization of long-circulating esterase-

responsive prodrug nanocarriers for bufalin in the treatment of esophageal cancer and prevention of metastasis are associated with remarkable efficacy. Notwithstanding, our group will conduct further in vivo pharmacodynamic study of PSNs in subsequent experiments for wider clinical applications of BFL in cancer treatment.

Conclusions

In summary, BFL exhibited a significant inhibitory effect on the proliferation, migration and invasion capabilities of KYSE150 cells. An ester prodrug was formed successfully with linoleic acid, wherein it possessed the ability to self-assemble into nanoparticles. After PEGylation modification, the stability and enzymatic degradation rate of the prodrug improved significantly. Additionally, different feed ratios of the prodrug and PEG had important impacts on stability and enzymatic degradation rate, with the 8:2 mass ratio demonstrating optimal stability and enzymatic degradation rate. Furthermore, the differences in stability and enzymatic degradation rate affected the inhibitory capabilities of the prodrug on KYSE150 cell proliferation, migration and invasion, with the 8:2 mass ratio showing the best effects. Therefore, our findings may contribute to the development of a BFL nanoparticle prodrug delivery system for clinical treatment of esophageal cancer.

Acknowledgment

Support for this work was given by Natural Science Foundation of China (Grant No.82104104) and School-level research projects of Yancheng Institute of Technology (grant no. xjr2020018, XJ201719).

Disclosure

The authors report no competing interest in this work.

References

1. Miao L, Liu Y, Ali NM, et al. Bufalin serves as a pharmaceutic that mitigates drug resistance. *Drug Metab Rev*. 2023;55(3):195–204. doi:10.1080/03602532.2023.2206065
2. Soumoy L, Ghanem GE, Saussez S, Journe F. Bufalin for an innovative therapeutic approach against cancer. *Pharmacol Res*. 2022;184:106442. doi:10.1016/j.phrs.2022.106442
3. Yin P-H, Liu X, Qiu -Y-Y, et al. Anti-tumor activity and apoptosis-regulation mechanisms of bufalin in various cancers: new hope for cancer patients. *Asian Pac J Cancer Preven*. 2012;13(11):5339–5343. doi:10.7314/APJCP.2012.13.11.5339
4. Lan YL, Lou JC, Jiang X W, et al. A research update on the anticancer effects of bufalin and its derivatives. *Oncol Lett*. 2019;17(4):3635–3640. doi:10.3892/ol.2019.10062
5. Chen G, Zhang H, Sun H, et al. Bufalin targeting BFAR inhibits the occurrence and metastasis of gastric cancer through PI3K/AKT/mTOR signal pathway. *Apoptosis*. 2023;28(9–10):1390–1405. doi:10.1007/s10495-023-01855-z
6. Yuan Z, Liu C, Sun Y, et al. Bufalin exacerbates photodynamic therapy of colorectal cancer by targeting SRC-3/HIF-1α pathway. *Int J Pharmaceut*. 2022;624:122018. doi:10.1016/j.ijpharm.2022.122018
7. Ding L, Yang Y, Lu Q, et al. Bufalin inhibits tumorigenesis, stemness, and epithelial–mesenchymal transition in colorectal cancer through a C-Kit/Slug signaling axis. *Int J Mol Sci*. 2022;23(21):13354. doi:10.3390/ijms232113354
8. Chen YY, Lu HF, Hsu SC, et al. Bufalin inhibits migration and invasion in human hepatocellular carcinoma SK-Hep1 cells through the inhibitions of NF-kB and matrix metalloproteinase-2/-9-signaling pathways. *Environ Toxicol Phar*. 2015;30(1):74–82. doi:10.1002/tox.21896
9. Fu R, Yu F, Wu W, et al. Bufalin enhances the killing efficacy of NK cells against hepatocellular carcinoma by inhibiting MICA shedding. *Int Immunopharmacol*. 2021;101:108195. doi:10.1016/j.intimp.2021.108195
10. Yu Z, Li Y, Li Y, et al. Bufalin stimulates antitumor immune response by driving tumor-infiltrating macrophage toward M1 phenotype in hepatocellular carcinoma. *J Immunother Cancer*. 2022;10(5):e004297. doi:10.1136/jitc-2021-004297
11. Wang H, Zhang C, Chi H, Meng Z. Synergistic anti-hepatoma effect of bufalin combined with sorafenib via mediating the tumor vascular microenvironment by targeting mTOR/VEGF signaling. *Int J Oncol*. 2018;52(6):2051–2060. doi:10.3892/ijo.2018.4351
12. Huang H, Lin X-J, Lin Y, Yao R-X, M-q H. Bufalin enhances the cytotoxity of human multiple myeloma cells H929 to AKT inhibitor MK2206: the role of protein AKT phosphorylation. *Indian J Hematol Blo*. 2018;34(2):268–272. doi:10.1007/s12288-017-0883-z
13. Liu F, Tong D, Li H, et al. Bufalin enhances antitumor effect of paclitaxel on cervical tumorigenesis via inhibiting the integrin α2/β5/FAK signaling pathway. *Oncotarget*. 2016;7(8):8896–8907. doi:10.18632/oncotarget.6840
14. Cheng CS, Wang J, Chen J, et al. New therapeutic aspects of steroidal cardiac glycosides: the anticancer properties of huachansu and its main active constituent bufalin. *Can Cell Inter*. 2019;19(1):92. doi:10.1186/s12935-019-0806-1
15. Zhang W, Fan Y, Zhang J, et al. Cell membrane-camouflaged bufalin targets NOD2 and overcomes multidrug resistance in pancreatic cancer. *Drug Resist Update*. 2023;71:101005. doi:10.1016/j.drup.2023.101005
16. Gao L, Zhang L, He F, et al. Surfactant assisted rapid-release liposomal strategies enhance the antitumor efficiency of bufalin derivative and reduce cardiotoxicity. *Int J Nanomed*. 2021;16:3581–3598. doi:10.2147/IJN.S313153
17. Hong X, Cai Z, Zhou F, et al. Improved pharmacokinetics of tenofovir ester prodrugs strengthened the inhibition of HBV replication and the rebalance of hepatocellular metabolism in preclinical models. *Front Pharmacol*. 2022;13:932934. doi:10.3389/fphar.2022.932934

18. Mazumder K, Hossain ME, Aktar A, et al. In silico analysis and experimental evaluation of ester prodrugs of ketoprofen for oral delivery: with a view to reduce toxicity. *Processes*. 2021;9(12):2221. doi:10.3390/pr9122221
19. Jornada DH, Dos Santos Fernandes GF, Chiba DE, et al. The prodrug approach: a successful tool for improving drug solubility. *Molecules*. 2015;21 (1):42. doi:10.3390/molecules21010042
20. Xiang J, Liu J, Liu X, et al. Enzymatic drug release cascade from polymeric prodrug nanoassemblies enables targeted chemotherapy. *J Control Release*. 2022;348:444–455. doi:10.1016/j.jconrel.2022.06.007
21. Liu T, Yuan X, Jia T, et al. Polymeric prodrug of bufalin for increasing solubility and stability: synthesis and anticancer study in vitro and in vivo. *Int J Pharmaceut*. 2016;506(1–2):382–393. doi:10.1016/j.ijpharm.2016.04.041
22. Li Y, Ye C, Cai C, et al. Design and synthesis of polymer prodrugs for improving water-solubility, pharmacokinetic behavior and antitumor efficacy of TXA9. *Pharm Res-DORDR*. 2020;37(3):1–14. doi:10.1007/s11095-020-02789-w
23. Dong H, Pang L, Cong H, Shen Y, Yu B. Application and design of esterase-responsive nanoparticles for cancer therapy. *Drug Deliv*. 2019;26 (1):416–432. doi:10.1080/10717544.2019.1588424
24. Yang L, Xu J, Xie Z, et al. Carrier-free prodrug nanoparticles based on dasatinib and cisplatin for efficient antitumor in vivo. *Asian J Pharm Sci*. 2021;16(6):762–771. doi:10.1016/j.ajps.2021.08.001
25. Zhang H, Wei S, Zhang Y, et al. Improving cellular uptake and bioavailability of periplocymarin-linoleic acid prodrug by combining PEGylated liposome. *Drug Deliv*. 2022;29(1):2491–2497. doi:10.1080/10717544.2022.2104406
26. Wang X, Yang B, Li L, et al. Probing the fluorination effect on the self-assembly characteristics, in vivo fate and antitumor efficacy of paclitaxel prodrug nanoassemblies. *Theranostics*. 2021;11(16):7896–7910. doi:10.7150/thno.61337
27. Zhang H-Y, C-y S, Adu-Frimpong M, J-n Y, X-m X. Glutathione-sensitive PEGylated curcumin prodrug nanomicelles: preparation, characterization, cellular uptake and bioavailability evaluation. *Int J Pharmaceut*. 2019;555:270–279. doi:10.1016/j.ijpharm.2018.11.049
28. Wang J, Matayoshi E. Solubility at the molecular level: development of a Critical Aggregation Concentration (CAC) assay for estimating compound monomer solubility. *Pharm Res-DORDR*. 2012;29(7):1745–1754. doi:10.1007/s11095-012-0730-8
29. Meewan J, Somani S, Almowalad J, et al. Preparation of zein-based nanoparticles: nanoprecipitation versus microfluidic-assisted manufacture, effects of PEGylation on nanoparticle characteristics and cellular uptake by melanoma cells. *Int J Nanomed*. 2022;17:2809–2822. doi:10.2147/IJN.S366138
30. Wang Q, Liang Q, Dou J, et al. Breaking through the basement membrane barrier to improve nanotherapeutic delivery to tumours. *Nat Nanotechnol*. 2023. doi:10.1038/s41565-023-01498-w
31. Wang H, Chen J, Xu C, et al. Cancer nanomedicines stabilized by π-π stacking between heterodimeric prodrugs enable exceptionally high drug loading capacity and safer delivery of Drug combinations. *Theranostics*. 2017;7(15):3638–3652. doi:10.7150/thno.20028
32. Li Y, Li L, Jin Q, et al. Impact of the amount of PEG on prodrug nanoassemblies for efficient cancer therapy. *Asian J Pharm Sci*. 2022;17 (2):241–252. doi:10.1016/j.ajps.2022.02.002
33. Suk JS, Xu Q, Kim N, Hanes J, Ensign LM. PEGylation as a strategy for improving nanoparticle-based drug and gene delivery. *Adv Drug Deliv Rev*. 2016;99(Pt A):28–51. doi:10.1016/j.addr.2015.09.012
34. Yang Y-H, Aloysius H, Inoyama D, Chen Y, L-q H. Enzyme-mediated hydrolytic activation of prodrugs. *Acta Pharm Sin B*. 2011;1(3):143–159. doi:10.1016/j.apsb.2011.08.001
35. Tian C, Guo J, Miao Y, et al. Triglyceride-mimetic structure-gated prodrug nanoparticles for smart cancer therapy. *J Med Chem*. 2021;64 (21):15936–15948. doi:10.1021/acs.jmedchem.1c01328
36. Kirpotin DB, Hayes ME, Noble CO, et al. Drug stability and minimized acid-/drug-catalyzed Phospholipid degradation in liposomal irinotecan. *J Pharm Sci-US*. 2023;112(2):416–434. doi:10.1016/j.xphs.2022.11.025
37. Huang R, Carney RP, Ikuma K, Stellacci F, Lau BL. Effects of surface compositional and structural heterogeneity on nanoparticle–protein interactions: different protein configurations. *ACS nano*. 2014;8(6):5402–5412. doi:10.1021/nn501203k
38. Liang P, Zhang Y, Schmidt BF, et al. Esterase-activated, pH-responsive, and genetically targetable nano-prodrug for cancer cell photo-ablation. *Small*. 2023;19(19):2207535. doi:10.1002/smll.202207535
39. Xia KS, Li DD, Wang CG, et al. An esterase-responsive ibuprofen nano-micelle pre-modified embryo derived nucleus pulposus progenitor cells promote the regeneration of intervertebral disc degeneration. *Bioact Mater*. 2023;21:69–85. doi:10.1016/j.bioactmat.2022.07.024
40. D-Z X, Sun X-Y, Liang Y-X, et al. Esterase-responsive polymeric micelles containing tetraphenylethene and poly(ethylene glycol) moieties for efficient doxorubicin delivery and tumor therapy. *Bioconjugate Chem*. 2023;34(1):248–256. doi:10.1021/acs.bioconjchem.2c00545
41. Wang X-W, Yang Z-Y, Li T, et al. Verteporfin exerts anticancer effects and reverses resistance to paclitaxel via inducing ferroptosis in esophageal squamous cell cancer cells. *Mol Biotechnol*. 2023. doi:10.1007/s12033-023-00891-z
42. Shim N, Jeon SI, Yang S, et al. Comparative study of cathepsin B-cleavable linkers for the optimal design of cathepsin B-specific doxorubicin prodrug nanoparticles for targeted cancer therapy. *Biomaterials*. 2022;289:121806. doi:10.1016/j.biomaterials.2022.121806
43. Yan F, Zhang C, Zheng Y, et al. The effect of poloxamer 188 on nanoparticle morphology, size, cancer cell uptake, and cytotoxicity. *Nanomed-Nanotechnol*. 2010;6(1):170–178. doi:10.1016/j.nano.2009.05.004
44. Zahednezhad F, Mojarrad JS, Zakeri-Milani P, et al. Surface modification with cholesteryl acetyl carnitine, a novel cationic agent, elevates cancer cell uptake of the PEGylated liposomes. *Int J Pharmaceut*. 2021;609:121148. doi:10.1016/j.ijpharm.2021.121148
45. Yang W, Wang L, Fang M, et al. Nanoparticle surface engineering with heparosan polysaccharide reduces serum protein adsorption and enhances cellular uptake. *Nano lett*. 2022;22(5):2103–2111. doi:10.1021/acs.nanolett.2c00349
46. Yang G, Liu Y, Hui Y, et al. Implications of quenching-to-dequenching switch in quantitative cell uptake and biodistribution of dye-labeled nanoparticles. *Angew Chem Int Edit*. 2021;60(28):15426–15435. doi:10.1002/anie.202101730
47. Wang H, Zhou W, Fu J, et al. Research on the mechanism of bufalin inhibiting migration and invasion of human prostate cancer PC3 cells. *Acta Pharma Sin*. 2022;57(5):1361–1366.
48. Guo C, Yuan H, Wang Y, et al. The interplay between PEGylated nanoparticles and blood immune system. *Adv Drug Deliv Rev*. 2023;200:115044. doi:10.1016/j.addr.2023.115044
49. Liu T, Li L, Wang S, et al. Hybrid chalcogen bonds in prodrug nanoassemblies provides dual redox-responsivity in the tumor microenvironment. *Nat Commun*. 2022;13(1):7228. doi:10.1038/s41467-022-35033-7